Ultra-High-Field MAS NMR Assay of a Multispin Labeled Ligand Bound to Its G-Protein Receptor Target in the Natural Membrane Environment: Electronic Structure of the Retinylidene Chromophore in Rhodopsin†

Michiel A. Verhoeven,‡ Alain F. L. Creemers,‡ Petra H. M. Bovee-Geurts,§ Willem J. De Grip,‡,§ Johan Lugtenburg,‡ and Huub J. M. de Groot*,‡

Leiden Institute of Chemistry, Gorlaeus Laboratories, Leiden University, P.O. Box 9502, NL-2300 RA Leiden, The Netherlands, and Department of Biochemistry and Institute of Cellular Signaling, University of Nijmegen, P.O. Box 9101, NL-6500 HB Nijmegen, The Netherlands

Received October 13, 2000; Revised Manuscript Received January 16, 2001

ABSTRACT: 11-*Z*-[8,9,10,11,12,13,14,15,19,20-$^{13}C_{10}$]Retinal prepared by total synthesis is reconstituted with opsin to form rhodopsin in the natural lipid membrane environment. The ^{13}C shifts are assigned with magic angle spinning NMR dipolar correlation spectroscopy in a single experiment and compared with data of singly labeled retinylidene ligands in detergent-solubilized rhodopsin. The use of multispin labeling in combination with 2-D correlation spectroscopy improves the relative accuracy of the shift measurements. We have used the chemical shift data to analyze the electronic structure of the retinylidene ligand at three levels of understanding: (i) by specifying interactions between the ^{13}C-labeled ligand and the G-protein-coupled receptor target, (ii) by making a charge assessment of the protonation of the Schiff base in rhodopsin, and (iii) by evaluating the total charge on the carbons of the retinylidene chromophore. In this way it is shown that a conjugation defect is the predominant ground-state property governing the molecular electronics of the retinylidene chromophore in rhodopsin. The cumulative chemical shifts at the odd-numbered carbons ($\Delta\sigma_{odd}$) of 11-*Z*-protonated Schiff base models relative to the unprotonated Schiff base can be used to measure the extent of delocalization of positive charge into the polyene. For a series of 11-*Z*-protonated Schiff base models and rhodopsin, $\Delta\sigma_{odd}$ appears to correlate linearly with the frequency of maximum visible absorption. Since rhodopsin has the largest value of $\Delta\sigma_{odd}$, the data contribute to existing and converging spectroscopic evidence for a complex counterion stabilizing the protonated Schiff base in the binding pocket.

Rhodopsin is the G-protein-coupled photoreceptor protein in the retina of vertebrates that initiates the visual signal transduction cascade in dim light vision. It is considered a paradigm for the superfamily of seven transmembrane helix G-protein-coupled receptors (GPCRs)[1] which comprises a physiologically widespread and pharmacologically very significant class of signal mediators (*1*−*4*). GPCRs trigger a wide variety of physiological processes that involve signaling by neurotransmitters, hormones, and neuropeptides. They are the major pharmaceutical targets for pharmacological intervention in human pathology. Characterization of the electronic structure of the ground state of ligands bound to their receptor targets will help to reveal the molecular mechanisms of receptor activation, thus facilitating identification of pharmacophores and improving drug design. The ligand in rhodopsin is 11-*Z*-retinal that is covalently bound to the protein via a protonated Schiff base (PSB) linkage with lysine residue 296 to form the retinylidene chromophore (Figure 1A). Upon absorption of a photon, the C11═C12 bond of the retinylidene ligand isomerizes from the 11-*Z* to the all-*E* configuration (*5*, *6*).

In recent years, rhodopsin has been studied in detail with MAS NMR techniques (*7*−*12*). The chemical shifts of the carbons in the polyene of the retinylidene ligand have been probed in a series of experiments using mono-^{13}C-labeled preparations (*7*). In such an approach, each experiment involves labeling of retinal with a ^{13}C isotope at a single predetermined position by chemical total synthesis, followed by isolation of the synthetic 11-*Z* isomer from the mixture of retinal isomers. After reconstitution of the singly labeled retinal into opsin to form rhodopsin, the MAS NMR response of the ^{13}C isotope can be measured. The rate-limiting step in this approach is the need for development of efficient total synthesis schemes for site-specific labeling. The few examples where this tedious scheme has been applied have taken more than a decade, which is an unrealistic time scale for routine studies of ligand−protein interactions.

Recent developments in the field of MAS NMR have provided broad-band dipolar recoupling techniques that can

† This research was supported by grants from Chemical Research Section of The Netherlands Organization for Advanced and Pure Research (NWO-CW) to J.L. (346-006). H.J.M.d.G. is a recipient of a PIONIER award of NWO-CW.

* To whom correspondence should be addressed. E-mail: h.groot@leidenuniv.nl. Fax: +31-71-5274603. Telephone: +31-71-5274539.

‡ Leiden University.

§ University of Nijmegen.

[1] Abbreviations: CP, cross polarization; FID, free induction decay; GPCR, G-protein-coupled receptor; HPLC, high-performance liquid chromatography; MAS, magic angle spinning; NMR, nuclear magnetic resonance; SB, Schiff base; PSB, protonated Schiff base; RFDR, radio-frequency-driven dipolar recoupling; TMS, tetramethylsilane; TPPM, two-pulse phase modulation; ν_{max}, frequency of maximum visible absorption.

10.1021/bi0023798 CCC: $20.00
Published on Web 02/17/2001

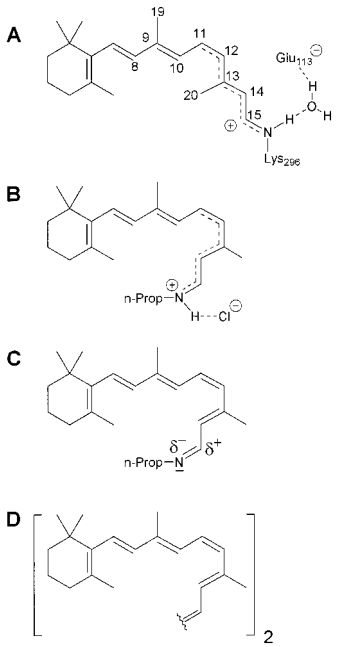

FIGURE 1: Chemical structures of the four retinoid species discussed in this study: (A) the chromophore in rhodopsin (the numbers indicate the position of the ^{13}C labels), (B) the 11-*Z*-PSB *N*-(11-*Z*-retinylidene)propyliminium chloride as in solution, (C) the corresponding 11-*Z*-SB, as in solution, and (D) 11-*Z*-β-carotene as in solution.

be applied in 2-D correlation experiments (*13*, *14*). These new techniques were recently used to detect, and partially assign, correlation signals from a multispin labeled pheophytin cofactor that was prepared via biosynthetic methods and incorporated into a 125 kDa photosynthetic reaction center membrane−protein complex (*15*). One purpose of this study is to demonstrate that MAS NMR dipolar correlation spectroscopy on a synthetically prepared multispin labeled retinal incorporated in opsin in its natural membrane environment can be used for a complete assignment of a predetermined multispin cluster, providing a MAS NMR shift image for characterization of the electronic structure in a single 2-D experiment. This sets the stage for creating chemical shift assays of the interaction of a ligand with its G-protein-coupled receptor target in the natural membrane environment. The utility of such images is illustrated with an assay of the electronic structure of the retinylidene group. We interpret the shift pattern in terms of a positive polaron-like conjugation defect stabilized by a negative complex counterion for the Schiff base (SB) environment in the active site of this GPCR.

MATERIALS AND METHODS

To incorporate a multispin cluster in the chromophore in rhodopsin, an efficient and cost-effective synthetic scheme was developed. The specific aim of this investigation is to incorporate the ^{13}C labels in the polyene part of the retinal toward the SB end. In that part the photoisomerization takes place, and the positive charge of the chromophore in the ground state is established by protonation of the SB nitrogen. To probe this region [8,9,10,11,12,13,14,15,19,20-$^{13}C_{10}$]-retinal was synthesized from natural abundance β-cyclocitral and the $^{13}C_5$-labeled building block [1,2,3,4,(3-methyl)-$^{13}C_5$]-3-methyl-4-(diethylphosphono)-2-butenitrile that contains the recurring segment in the polyene (*16*). In Figure 1A the ^{13}C-label positions are indicated with their respective number. The purified mixture of configurational retinal isomers obtained by synthesis was irradiated in acetonitrile to generate the 11-*Z* isomer in a maximum amount. The 11-*Z* isomer was separated from this mixture by straight-phase HPLC (silica gel, 1.2 × 25 cm; Dupont) (*17*).

Retinas were dissected from approximately 50 fresh cow eyes within 4 h after slaughter. Bleached membrane fragments containing opsin, the apoprotein of rhodopsin, were isolated and regenerated with a ~3-fold excess of the 11-*Z*-$^{13}C_{10}$-retinal following published procedures (*18*). Excess of retinal was removed by extraction with β-cyclodextrin (*19*). Incorporation was checked by optical spectroscopy; the observed (A_{280}/A_{500}) ratio was 2.0, corresponding with an incorporation level of the labeled retinal of more than 90%. The rhodopsin sample containing the multiply labeled chromophore was concentrated by centrifugation and loaded into a 4 mm zirconium oxide rotor and sealed with a Kel-F cap. CP/MAS spectra were recorded with a Bruker DSX-750 spectrometer operating at a ^{13}C frequency of 188 MHz and equipped with a 4 mm MAS probe. Ramped cross-polarization (*21*) with a contact time of 2.0 ms and the TPPM decoupling scheme (*22*) were used. The sample was cooled with nitrogen gas at a temperature of 223 K. The 1-D spectrum was recorded using a MAS frequency of 12.000 Hz ± 3 Hz, and the cycle time between scans was 2 s. Prior to Fourier transformation the FID arrays were zero-filled to 2K points, and an exponential line-broadening function of 50 Hz was applied. 2-D RFDR spectra were also recorded using a MAS frequency of 12.000 ± 3 Hz and a mixing time $\tau_m = 2.67$ ms, while during mixing CW decoupling was used with a nutation frequency of 83 kHz. In the t_1 domain 200 slices with 10 μs increment were collected, and for each slice 480 transients were recorded in the t_2 domain. TPPM decoupling was used during acquisition, and the cycle time between scans was 2 s. Prior to double Fourier transformation the t_2 dimension was zero-filled to 2K points, and an exponential line-broadening function of 75 Hz was applied. Zero-filling in t_1 was to 512 points, and a quadratic sine apodization window shifted by $2.7/\pi$ was applied. Chemical shifts are reported relative to TMS, using the shift that was determined previously for C-11 as internal references (*11*).

To calculate the chemical shift differences, ^{13}C NMR data for the PSB model *N*-(11-*Z*-retinylidene)propyliminium chloride (Figure 1B) (*23*), the SB model *N*-(11-*Z*-retinylidene)propylimine (Figure 1C) (*23*), and 11-*Z*-β-carotene (Figure 1D) (*24*) in solution were taken from the literature (Table 2). Data for two 11-*Z*-PSB salts, *N*-(11-*Z*-retinylidene)propyliminium trifluoroacetate and bromide, in Figure 5, were taken from refs *23* and *25*, respectively. The crystal structure data of two all-*E* PSB salts, *N*-(all-*E*-retinylidene)-*tert*-butyliminium perchlorate and triflate, used in the discussion are from ref *26*.

RESULTS

The 1-D spectrum of rhodopsin reconstituted with the 10-fold ^{13}C-labeled retinal (Figure 1A) is shown in Figure 2A, while Figure 2B gives the natural abundance ^{13}C spectrum of native rhodopsin. In the spectrum of native rhodopsin the natural abundance ^{13}C nuclei of the saturated carbons including the aliphatic carbons of the amino acid side chains

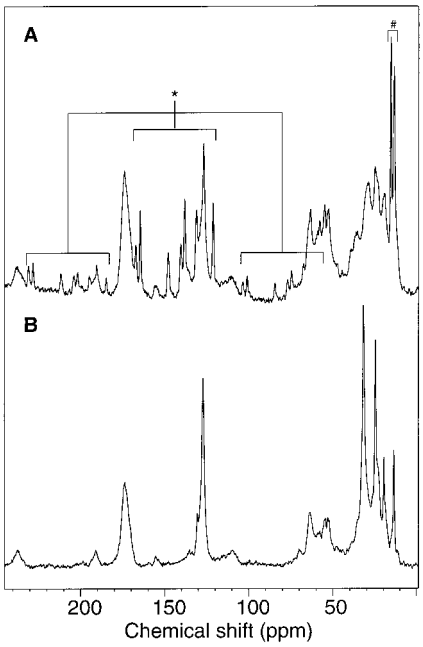

FIGURE 2: (A) Proton-decoupled ^{13}C CP/MAS spectra of rhodopsin containing a 10-fold ^{13}C-labeled retinylidene chromophore. The center-band region of the vinylic carbons (*) and the spinning side-band regions on both sides are indicated. The resonances of the methyl groups 19 and 20 are also indicated (#). (B) The spectrum of native rhodopsin shows the natural abundance ^{13}C signals of the protein and natural phospholipid membrane. The carbonyl signals of protein and phospholipids are found at ~175 ppm, saturated carbons of phospholipids and aromatic amino acid residues resonate with ~127 ppm, and aliphatic signals are observed upfield at 0−70 ppm. The spectra were recorded with the same instrument settings with a temperature of 223 K and with a spinning frequency of 12.000 Hz ± 3 Hz.

of the protein and membrane phospholipids resonate between 0 and 70 ppm. At ~127 ppm the natural abundance response from the unsaturated carbons in the phospholipids and aromatic carbons in the protein residues is observed. Finally, the broad signal around 175 ppm is a superposition of the peptide carbonyl and lipid ester response. The spectrum of rhodopsin with the 10-fold labeled retinylidene ligand shows additional sharp resonances of the center bands and side bands of the enriched carbon nuclei in the retinylidene chromophore. For instance, the two strong signals in the aliphatic region at 13.8 and 15.8 ppm are the resonances from the C-19 and C-20 methyl groups (Table 1). These signals do not show spinning side bands, due a small shift anisotropy ($|\sigma_{11}|$ and $|\sigma_{33}| \ll \omega_r$) of these sp^3 hybrid atoms. In the vinylic region the eight remaining center-band signals are detected. Seven signals are well resolved with isotropic shifts between 120 and 170 ppm. A response around 128 ppm is superimposed on the natural abundance response of the phospholipids. This label signal can be assigned unambiguously by its spinning side band at 191 ppm, since the anisotropy of the phospholipid signals is relatively small and the side-band signal in this region is weak (cf. Figure 2B). The chemical shifts for the resolved resonances of the labeled positions in the retinylidene suggest an NMR response analogous to signals previously reported by Smith et al. (Table 1) (*7*). However, a correlation experiment is needed to arrive at an unambiguous assignment of all resonances of the multispin labeled ligand.

Table 1: Isotropic ^{13}C MAS NMR Shifts for the Labeled Positions in the 10-fold ^{13}C-Labeled Retinylidene Chromophore of Rhodopsin in the Native Membrane Obtained in a Direct Approach Using Homonuclear Correlation Spectroscopy (Figure 3)[a]

carbon	rhodopsin in native membrane	rhodopsin in Ammonyx-LO[b]	$\Delta\sigma$
8	138.5	139.2	−0.7
9	148.2	148.5	−0.3
10	127.2	127.8	−0.6
11	140.8	141.6	−0.8
12	131.5	132.1	−0.6
13	167.6	168.9	−1.3
14	121.6	121.2	0.4
15	165.0	165.4	−0.4
19	13.8	12.0	+1.8
20	15.8	16.8	−1.0

[a] The shifts are compared with the ^{13}C shift collected in a stepwise approach using rhodopsins solubilized in detergent (Ammonyx-LO). [b] Data from ref *7*.

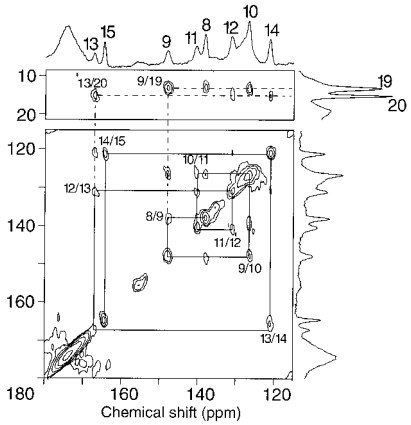

FIGURE 3: Detail of the contour plot of the ^{13}C MAS 2-D dipolar correlation spectrum collected from rhodopsin reconstituted with a 10-fold ^{13}C-labeled retinal. The data are recorded at 223 K and with a spinning frequency of 12.000 Hz ± 3 Hz. The solid lines indicate the correlation network of the ^{13}C-labeled carbons in the polyene, and the dashed lines indicate the connectivities with the methyl groups. The complete assignment of the carbons is indicated in the projection.

The incorporation of a multispin ^{13}C cluster gives the possibility to assign the NMR response with broad-band dipolar correlation spectroscopy. To assign all ^{13}C-labeled carbons in a single experiment, we have performed 2-D RFDR dipolar correlation spectroscopy with simulated phase-sensitive detection in t_1 (*27*). This approach is easy to implement, and it has been shown in experimental and theoretical studies that it is much more broad band than originally thought (*27*, *28*). In particular, in practical cases it provides strong correlation signals when the chemical shift differences are small, i.e., cross-peaks close to the diagonal in the 2-D experiment. The connectivities between adjacent ^{13}C isotopes that are obtained with the 2-D spectrum shown in Figure 3 confirm the utility of the phase-sensitive RFDR experiment for the assignment of olefinic carbons with small chemical shift dispersion in the solid state and lead to a complete assignment of the signals from the labels (Table 1). Additional weak correlations reveal some relayed magnetization transfer in the multispin ^{13}C network, and they support the assignments listed in Table 1. The chemical shift measurements obtained with a multispin labeled cluster in the retinylidene have a relative precision of ~0.1 ppm, considerably better than the ~1 ppm reported for the data

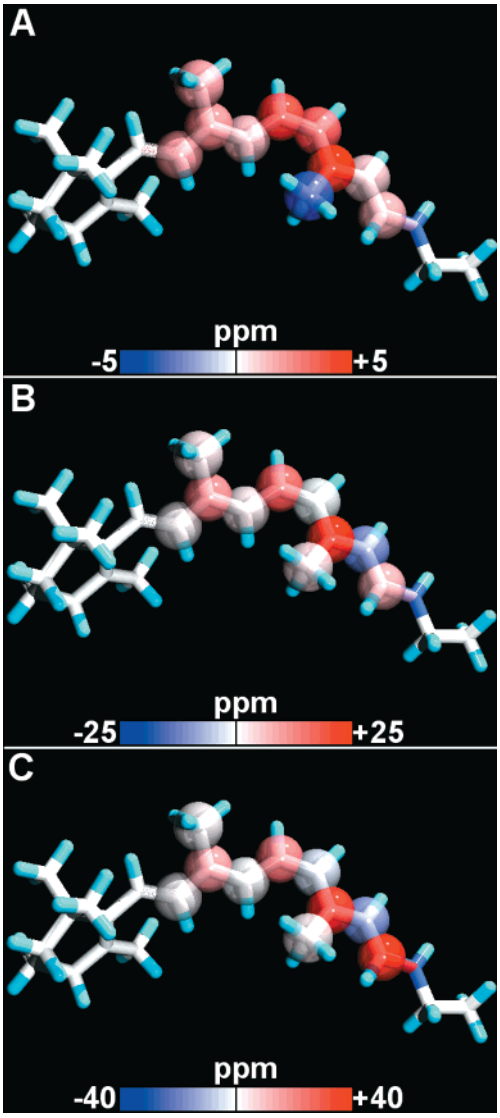

FIGURE 4: MAS NMR shift images of the retinylidene chromophore in rhodopsin. The structural model is taken from ref *31*. The $\Delta\sigma$ are indicated with translucent spheres around the atom. Blue and red indicate upfield and downfield shifts, respectively, and the larger the shift the darker the color. (A) Difference $\Delta\sigma_{PSB}$ between rhodopsin and PSB model *N*-(11-*Z*-retinylidene)propyliminium chloride. (B) Difference $\Delta\sigma_{SB}$ between rhodopsin and the analogue SB. (C) Difference $\Delta\sigma_{Car}$ between rhodopsin and the 11-*Z*-carotene. The shift differences correspond with Table 2.

collected from the specifically labeled retinals that were used in a stepwise serial approach (*8*).

DISCUSSION

The multispin labeling and the assignment of the ^{13}C signals from dipolar correlation spectroscopy on the multispin cluster can be used to resolve essential details of the electronic structure of the ligand in the G-protein-coupled receptor target in a single experiment. In Figure 4 three different schemes are presented for translating the chemical shift information into a MAS NMR shift image using color-encoded spheres around the labeled carbon atoms. The size of the spheres corresponds with 0.85 Å, which is equal to half the van der Waals radius of carbon (*29*). In rhodopsin the chromophore carries a full positive charge, due to the protonation of the SB nitrogen (Figure 1A).

Table 2: Chemical Shift Differences for the 11-*Z*-PSB in Rhodopsin Relative to the Model Compounds 11-*Z*-PSB ($\Delta\sigma_{PSB}$), 11-SB ($\Delta\sigma_{SB}$), and 11-*Z*-β-Carotene ($\Delta\sigma_{Car}$)

carbon	$\Delta\sigma_{PSB}$[a]	$\Delta\sigma_{SB}$[a]	$\Delta\sigma_{Car}$[b]
8	1.3	0.5	0.7
9	1.6	8.9	11.2
10	0.8	0.9	0.1
11	3.3	13.1	15.7
12	2.5	−0.2	−2.1
13	4.9	22.6	31.2
14	0.3	−8.4	−11.4
15	1.1	5.4	35.0
19	1.4	1.6	1.0
20	−3.0	−1.9	−1.5

[a] Data on the PSB and SB from ref *23*. [b] Data on carotene from ref *24*.

In Figure 4A the effect of the protein environment on the charge distribution is visualized. The difference between rhodopsin (Figure 1A) and the PSB model *N*-(11-*Z*-retinylidene)propyliminium chloride (Figure 1B) is represented by plotting the chemical shift differences $\Delta\sigma_{PSB} = \sigma_{Rho} - \sigma_{PSB}$ at each atom (Table 2). The corresponding effect on the ν_{max} is commonly referred to as the "opsin shift" (*30*). When the new assignment is compared with the earlier results, it transpires that the effect of the medium containing the protein on details of its electronic structure is small (Table 1). The chemical shifts of the polyene carbons agree with those reported for the series of single label experiments, essentially within its error margin of 1 ppm. The difference of 1.5 ppm for C-13 and the systematic deviation of the other carbons may, however, indicate slightly less positive charge polarization in the natural lipid environment compared to the rhodopsins in detergent (Table 1). The structure of the isomerization region of the retinylidene chromophore in rhodopsin has been determined at high resolution with MAS NMR distance measurements and Car−Parrinello ab initio density functional methods (*11*, *31*). The ligand is forced into a nonplanar 12-s-*trans* conformation by nonbonding steric constraints of the protein binding pocket. This structure is different from the more relaxed 12-s-*cis* conformation commonly observed for 11-*Z*-PSB models in solution (*32*, *33*). The upfield shift of C-20 relative to the PSB model is not yet explained in detail. The stabilization of additional positive charge at C-13 and the adjacent polyene carbons has been attributed before to mutual polarization effects between the polyene and the Glu_{113} (*7*, *8*). A recent X-ray model for rhodopsin confirms that Glu_{113} stabilizes the PSB in rhodopsin. However, in the X-ray model Glu_{113} is positioned somewhat closer to the PSB nitrogen than for a seminal 3-D structural model inferred from chemical shift constraints (*25*, *34*).

The shift differences $\Delta\sigma_{SB} = \sigma_{Rho} - \sigma_{SB}$ between rhodopsin and the unprotonated 11-*Z*-SB (Figure 1C) are visualized in Figure 4B. The more extended the delocalization of positive charge into the polyene, the more excess positive charge is stabilized on the odd-numbered atoms and the more downfield their chemical shift values. Hence, Figure 4B clearly shows that the chemistry of protonation of the SB involves delocalization of the positive charge into the polyene. In addition, there is an increase of charge density alternation between the odd- and even-numbered atoms at the SB end of the chromophore, which is reflected in downfield and upfield $\Delta\sigma_{SB}$. The positive charges on the odd-numbered lattice positions induce correlated negative charge

polarization on the even-numbered positions via the Coulomb interaction. As a general rule, the upfield shifts for the even-numbered carbons increase when the delocalization of the positive charge at the odd-numbered carbons is more pronounced (*35*).

Finally, we show in Figure 4C the difference $\Delta\sigma_{Car} = \sigma_{Rho} - \sigma_{Car}$ between corresponding carbons in rhodopsin and 11-*Z*-*β*-carotene (Figure 1D). This carotenoid represents an unpolarized reference compound with the characteristic structural properties of an 11-*Z* retinoid (Figure 1D). Presented in this way, the $\Delta\sigma_{Car}$ reveal the positively charged conjugation defect that was extensively discussed in recent literature (*31*, *36*−*40*). The conjugation defect is an emerging property with a half-width of about 3 bond lengths. It is autolocalized due to a balance between the energy gain associated with delocalization of the electrons involved, on one hand, and the energy cost due to the deformation of the underlying molecular frame. The defect is thermodynamically stable in the ground state and corresponds chemically with a region of enhanced nonbonding character and a nodal plane in the molecular electronic structure. The conjugation defect in the polyene of rhodopsin is thought to mediate the primary step in vision in a classically coherent dynamic process by increasing the effective mass of the electronic charge by 2 orders of magnitude. Its autolocalized nodal plane can be confined to the isomerization region and transferred over a carbon−carbon bond. In this scheme the *Z* to *E* isomerization process is driven by the necessity to preserve the overall bonding character in the retinylidene moiety and involves only very minor atomic displacements, mainly the transfer of a single H-12 to the opposite side of the C11═C12 bond (*31*, *36*, *41*). This mechanism is essentially different from a scheme that involves a significant motion of the C-13 methyl group or the H-10 driving the isomerization process by releasing nonbonding steric interaction, as has been inferred from linear extrapolation of excited-state surface motion upon photoexcitation (*42*). It is, however, in line with FTOA measurements that provide strong evidence that a motion of hydrogens attached to the C11═C12 double bond becomes predominant during photoisomerization at a time scale of more than 70 fs after photoexcitation (*43*).

The total amount of positive charge that is induced on the carbons in the retinylidene of rhodopsin can now be divided into three synergistic contributions: (1) polarization by the electronegative SB nitrogen, (2) protonation of the SB nitrogen, and (3) mutual polarization effects between the counterion and the protonated SB nitrogen. An approximately linear relation between ^{13}C shift difference and relative atomic charge density has been reported for conjugated systems (*44*−*46*). The cumulative changes $\Delta\sigma^{tot}$ for the observed polyene carbons listed in Table 2 can be translated into electronic charge density differences by using a conversion factor of +155 ppm/unit charge. In this way the total polarization associated with each of the three terms can be estimated. Comparing rhodopsin with the 11-*Z*-*β*-carotene, the $\Delta\sigma^{tot}_{Car}$ listed in the last column in Table 2 add up to 80.5 ppm. Hence the total amount of positive charge accumulated by the polyene carbons is approximately ∼0.5 electronic equivalent, which is mainly located on C-15 and C-13. This is an important observation, since it indicates that the center of the conjugation defect may be inside the polyene, in qualitative agreement with the theoretical predictions (*31*, *36*). Such a delocalized charge is expected to affect the C−C/C═C bond length alternation pattern, in the same way a polaronic exitation perturbs the polyene bond alternation pattern in an infinite conjugated chain (*47*, *48*). The coupling between electronic configuration and the underlying molecular framework in a polyene is particularly strong. A charge in a polyene perturbs the backbone locally and corresponds with a HOMO with nonbonding character that is self-localized and confined to a region in which the bond length alternation is reduced (*49*, *47*). In the case of rhodopsin such a perturbation causes that the double bond character of the C-15/N and C-13/C-14 will be reduced, while the C-14/C-15 bond will have increased double bond character. The delocalization of positive charge and the region in which the bond length alternation pattern is affected are schematically indicated in Figure 1A. Crystal structure data for PSB model compounds provide strong support for the concept of a decrease of bond length alternation due to charging. To detect the center of the conjugation defect in the polyene, the dimerization amplitudes (*50*)

$$D_{i,j,k} = d_{i,j} - d_{j,k} \quad (1)$$

can be calculated following ref *31*. Here $d_{i,j}$ and $d_{j,k}$ denote the bond lengths between atoms *i*,*j* and *j*,*k* of adjacent bonds. A conjugation defect is present in the polyene when a $D_{i,j,k}$ has the same sign as $D_{i+1,j+1,k+1}$. For instance, for all-*E*-*β*-carotene, without charge or polarization, the sign of the dimerization amplitude alternates over the entire polyene with $|D_{i,j,k}| \sim 0.15$ Å (*51*). This contrasts with high-resolution X-ray structural data obtained for PSB models *N*-(all-*E*-retinylidene)-*tert*-butyliminium perchlorate and triflate (*26*), which clearly show reduced bond length alternation with the smallest value of $D_{13,14,15} = -0.05$ Å at the SB end of the polyene chain. Since the electron−lattice interaction is generally the predominant interaction in polyenes, the results for the PSB models imply that a similar defect and associated decreased bond length alternation can be expected for the Schiff base in rhodopsin upon charging.

According to the values of $\Delta\sigma_{Car}$ in Table 2, the C-15 of the retinylidene in rhodopsin accumulates ∼0.23 electronic equivalent of positive charge, slightly more than the ∼0.20 equivalent on C-13. In addition, the total cumulative charge difference between the carbon atoms of rhodopsin and carotene appears not larger than ∼0.5 electronic equivalent. This suggests that the conjugation defect has not entirely moved into the carbon part of the polyene. It contrasts with theoretical calculations of the system in a vacuum, which put a conjugation defect between C-13 and C-15, as calculated from the sign pattern of the dimerization amplitude (*31*).

Protonation of the SB nitrogen also increases the amount of delocalized charge on the carbons. The shift pattern provides additional support for a conjugation defect located in the polyene close to the SB nitrogen, fully established by the protonation event. The excess charge injected into the polyene of rhodopsin by the protonation yields a total cumulative shift of 43.0 ppm, calculated from the $\Delta\sigma_{SB}$ in Table 2. This leads to the conclusion that an estimated ∼0.3 electronic equivalent out of the total of ∼0.5 calculated for the $\Delta\sigma^{tot}_{Car}$ is associated with the process of protonation in the binding site, measured by $\Delta\sigma^{tot}_{SB}$. It is a crucial

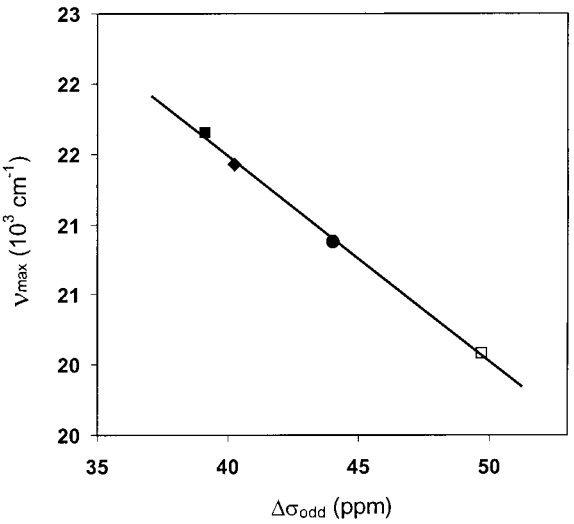

FIGURE 5: Relation between ν_{max} and $\Delta\sigma_{odd}$ for 11-*Z*-PSB salts with different counterions and rhodopsin. The line represents the linear least-squares fit to the points with $R^2 = 0.998$. The 11-*Z*-PSB salts are indicated with solid markers: *N*-(11-*Z*-retinylidene)-propylimine chloride, ref *23* (■); the trifluoroacetate ref *23* (◆); and the bromide, refs *25* and *12* (●). Rhodopsin is indicated with an open marker; values are from this work (□).

observation that this ~0.3 charge is mainly transferred to the C-11 and the C-13 and not to the C-15, fully in line with the concept of an autolocalized defect (Figure 4B). It also illustrates that the polarization due to the electronegative nitrogen in the SB provides a considerable contribution of ~0.2 electronic equivalent to the total amount of positive charge in the polyene (Figure 1C).

Recently, it was concluded from ^{15}N MAS NMR studies that the PSB in rhodopsin is stabilized by a complex counterion (*12*). This was based on a set of correlations between ^{15}N shift and the ν_{max} and between ν_{max} and the effective center−center distance between the counterion and the PSB nitrogen. The weaker the interaction between PSB and counterion, the more extended the delocalization of the positive charge from the protonated nitrogen into the polyene. The charge $\Delta\sigma^{tot}_{PSB}$ between the PSB in rhodopsin (Figure 1A) and the PSB model (Figure 1B) yield a moderate total shift of 15.9 ppm, corresponding with ~0.1 electronic equivalent. This is attributed to a complex counterion environment in the protein. The delocalization of positive charge over the polyene establishes a HOMO and LUMO, both with pronounced nonbonding character, well inside the gap between the π and π^* molecular orbital manifolds.

Protonation of the SB nitrogen and decreasing the counterion strength will give rise to an increase of the energy of the HOMO, accompanied by a decrease of the energy of the LUMO (*31*, *53*). It is thus interesting to search for a correlation between the HOMO−LUMO gap measured by the ν_{max} and the extent of the polarization into the polyene that is measured in our NMR experiment. This is most conveniently done by taking the 11-*Z* unprotonated SB as the reference compound (cf. Figure 4C). The extent of positive charge delocalization on the odd-numbered carbons due to protonation can be estimated for several 11-*Z*-6-*s*-*cis*-PSB models with different counterions by taking the cumulative shift difference of the odd-numbered carbons, $\Delta\sigma_{odd} = \Sigma(\sigma_{PSB,odd} - \sigma_{SB,odd})$. We find that $\Delta\sigma_{odd}$ is well correlated with ν_{max} (Figure 5). The shift difference at C-15 going from the SB to the 11-*Z*-PSB model or rhodopsin is small, and hence the C-15 has a small contribution to $\Delta\sigma_{odd}$. By consequence, $\Delta\sigma_{odd}$ mainly reflects differences at the C-13 and C-11. Thus, the correlation between ν_{max} and $\Delta\sigma_{odd}$ measures the extent of positive charge delocalization into the polyene. An approximate linear relation transpires after performing a linear least-squares fit according to

$$\nu_{max} = (-1.46 \times 10^2)(\Delta\sigma_{odd}) + 27.3 \times 10^3 \qquad (2)$$

Equation 2 fulfills the requirement of self-consistency that the offset 27.3×10^3 is nearly the same as the ν_{max} of 27.4×10^3 cm^{-1} of the SB, the uncharged point of reference. This confirms that the correlation is almost linear. Equation 2 encompasses rhodopsin, and compared to the PSB models, for rhodopsin a small HOMO−LUMO gap correlates with a large extent of positive charge delocalization. Since the data point for rhodopsin in Figure 5 is well outside the region spanned by the model compounds, our data provide strong evidence that the anion provided by the protein is very weak. This is an essential characteristic of some form of a complex counterion, fully in line with the analysis of recent ^{15}N MAS NMR measurements on rhodopsin (*12*). It is remarkable that both the decrease of charge measured by the nitrogen shift and the resulting increase of positive charge measured with the carbons shifts correlate with ν_{max}, which validates the use of both ^{15}N and ^{13}C shifts to probe the counterion strength. A relation between the ν_{max} and the effective center−center distance

$$d_{eff} = 24.17[\nu_{max} - (1.70 \times 10^4)]^{-1/2} \qquad (3)$$

between the centers of the counterion and the SB nitrogen was deduced for 11-*Z*- and all-*E*-PSBs in solution (*12*). Since $\Delta\sigma_{odd}$ also correlates with the ν_{max}, eq 3 yields an effective center−center distance of 0.43 nm of the ion pair in the active site of rhodopsin. In this way the ^{13}C MAS NMR contributes to converging spectroscopic evidence for a complex counterion stabilizing the PSB in rhodopsin. The effective distance of 0.43 nm is considerably larger than the ~0.34 nm proposed in the recently derived crystal structure model of rhodopsin (*33*). This suggests the presence of a hydrogen-bonded water molecule between the PSB and the carboxylate of Glu_{113} ($N^+-H\cdots OH_2\cdots O^-$) (*12*). In parallel, eqs 2 and 3 indicate that spectral tuning of rhodopsins and the cone pigments responsible for color vision, in the regime <500 nm, can be accomplished also by varying the anionic interactions exerted by the protein pocket in the vicinity of the PSB.

CONCLUSIONS

2-D solid-state NMR correlation data collected from rhodopsin reconstituted with synthetically prepared multispin labeled retinal can be used to assign the chemical shifts of the chromophore and to provide a MAS NMR shift image of the ligand−protein interactions and the electronic structure of the ligand. This direct method is much faster and considerably improves the relative precision of the shift measurements compared to the established method of using specifically labeled retinals in a serial approach. The ^{13}C chemical shifts observed for the carbons in the polyene of the chromophore in rhodopsin in its native lipid environment

are marginally different from the shifts determined for the detergent-solubilized system. It is illustrated how multispin labeling in combination with solid-state 2-D correlation spectroscopy can be a versatile method for assessment of ligand−protein interactions for GPCR targets and other membrane proteins. An analysis of the SB environment supports the model of stabilization of the protonation by a complex counterion. In addition, it is shown that the excess positive charge in the polyene is due to the three synergistic contributions: the electronegative nitrogen, the protonation, and the counterion strength. Finally, NMR analysis of the molecular electronics of the retinylidene chromophore reveals essential characteristics of a conjugation defect in the polyene of rhodopsin that is stable in the ground state.

ACKNOWLEDGMENT

We thank Johan Hollander, Cees Erkelens, and Fons Lefeber for assistance with the MAS NMR experiments.

REFERENCES

1. Watson, S., and Arkinstall, S. (1994) in *The G-Protein Linked Receptor Facts Book*, Academic Press, San Diego, CA.
2. Tang, L., Ebrey, T. G., and Subramaniam, S. (1995) *Isr. J. Chem. 35*, 193−209.
3. Pogozheva, I. R., Lomize, A. L., and Mosberg, H. I. (1997) *Biophys. J. 70*, 1963−1985.
4. Verdegem, P. J. E., Lugtenburg, J., and De Groot, H. J. M. (1997) in *Pharmacochemistry Library, Vol. 26, Stable Isotopes in Pharmaceutical Research* (Browne, T., R., and Timmerman, H., Eds.) Chapter 10, pp 2−14, Elsevier, Amsterdam.
5. Wald, G. (1962) *Science 162*, 230−239.
6. Hubbart, R., and Croft, A. (1958) *Proc. Natl. Acad. Sci. U.S.A. 44*, 130−139.
7. Smith, S. O., Palings, I., Miley, M. E., Courtin, J., De Groot, H. J. M., Lugtenburg, J., Mathies, R. A., and Griffin, R. G. (1990) *Biochemistry 29*, 8158−8164.
8. Smith, S. O., Courtin, J., De Groot, H. J. M., Gebhard, R., and Lugtenburg, J. (1991) *Biochemistry 30*, 7409−7415.
9. Smith, S. O., De Groot, H. J. M., Gebhard, R., and Lugtenburg, J. (1992) *Photochem. Photobiol. 56*, 1035−1039.
10. Feng, X., Verdegem, P. J. E., Lee, Y. K., Sandström, D., Edén, M., Bovee-Geurts, P., De Grip, W. J., Lugtenburg, J., De Groot, H. J. M., and Levitt, M. H. (1997) *J. Am. Chem. Soc. 119*, 6853−6857.
11. Verdegem, P. J. E., Bovee-Geurts, P. H. M., De Grip, W. J., Lugtenburg, J., and De Groot, H. J. M. (1999) *Biochemistry 38*, 11316−11324.
12. Creemers, A. F. L., Klaassen, C. H. W., Bovee-Geurts, P. H. M., Kelle, R., Kragl, U., Raap, J., De Grip, W. J., Lugtenburg, L., and De Groot, H. J. M. (1999) *Biochemistry 38*, 7195−7199.
13. Bennet, A. E., Ok, J. H., Griffin, R. G., and Vega, S. (1992) *J. Chem. Phys. 96*, 8624−8627.
14. Griffin, R. G. (1998) *Nat. Struct. Biol. 5* (Suppl. S), 508−512.
15. Egorova-Zachernyuk, T. A., Van Rossum, B.-J., Boender, G.-J., Franken, E., Ashurts, J., Raap, J., Gast, P., Hoff, A. J., Oschkinat, H., and De Groot, H. J. M. (1997) *Biochemistry 36*, 7513−7519.
16. Lugtenburg, J., Creemers, A. F. L., Verhoeven, M. A., Van Wijk, A. A. C., Verdegem, P. J. E., Monnee, M. C. F., and Jansen, F. J. H. M. (1999) *Pure Appl. Chem. 71*, 2245−2251.
17. Lugtenburg, J. (1985) *Pure Appl. Chem. 57*, 753−762.
18. De Grip, W. J., Deamen, F. J. M., and Bonting, S. L. (1980) *Methods Enzymol. 67*, 301−320.
19. De Lange, F., Bovee-Geurts, P. H. M., Van Oostrom, J., Portier, M. D., Verdegem, P. J. E., Lugtenburg, J., and De Grip, W. J. (1998) *Biochemistry 37*, 1411−1420.
20. De Lange, F., Bovee-Geurts, P. H. M., Van Oostrom, J., Portier, M. D., Verdegem, P. J. E., Lugtenburg, J., and De Grip, W. J. (1998) *Biochemistry 37*, 1411−1420.
21. Metz, G., Wu, X., and Smith, S. O. (1994) *J. Magn. Reson. A110*, 219−227.
22. Bennet, A. E., Rienstra, C. M., Auger, M., Lakshmi, K. V., and Griffin, R. G. (1995) *J. Chem Phys. 103*, 6951−6958.
23. Shriver, J. W., Mateescu, G. D., and Abrahamson, E. W. (1979) *Biochemistry 18*, 4785−4792.
24. Englert, G. (1995) in *Carotenoids, Volume 1B: Spectroscopy* (Britton, G., Liaaen-Jensen, S., and Pfander, H., Eds.), pp 212 and 224, Birkhäuser Verlag, Basel.
25. Han, M., DeDecker, B. S., and Smith, S. O. (1993) *Biophys. J. 65*, 899−906.
26. Elia, G. R., Childs, R. F., Britten, J. F., Yang, D. S. C., and Santasiero, B. D. (1996) *Can. J. Chem. 74*, 591−601.
27. Boender, G.-J., Raap, J., Prytulla, S., Oshkinat, H., and De Groot, H. J. M. (1995) *Chem. Phys. Lett. 237*, 502−507.
28. Boender, G.-J., Vega, S., and De Groot, H. J. M. (2000) *J. Chem. Phys. 112*, 1096−1106.
29. Bondi, A. (1964) *J. Phys. Chem. 68*, 441−451.
30. Nakanishi, K., Balogh-Nair, V., Arnaboldi, M., Tsjuimoto, K., and Honig, B. (1980) *J. Am. Chem. Soc. 102*, 7945−7947.
31. Buda, F., De Groot, H. J. M., and Bifone, A. (1996) *Phys. Rev. Lett. 77*, 4474−4477.
32. Albeck, A., Livnah, N., Gottlieb, H., and Sheves, M. (1992) *J. Am. Chem. Soc. 114*, 2400−2411.
33. Palczewski, K., Kumasaka, T., Hori, T., Behnke, C. A., Motoshima, H., Fox, B. A., Le Trong, I., Teller, D. C., Okada, T., Stenkamp, R. E., Yamamoto, M., and Miyano, M. (2000) *Science 289*, 739−745.
34. Han, M., and Smith, S. O. (1995) *Biochemistry 34*, 1425−1432.
35. Boudreaux, D. S., Chance, R. R., Brédas, J. L., and Silbey, R. (1983) *Phys. Rev. B28*, 258−267.
36. Bifone, A., De Groot, H. J. M., and Buda, F. (1997) *J. Phys. Chem. B 101*, 2954−2958.
37. Aalberts, D. P., Vos, F. L. J., and Van Saarloos W. (1997) *Pure Appl. Chem. 69*, 2099−2104.
38. Bifone A., de Groot, H. J. M., and Buda, F. (1997) *Pure Appl. Chem 69*, 2105−2110.
39. La Penna, G., Buda, F., Bifone, A., and De Groot, H. J. M. (1998) *Chem. Phys. Lett. 294*, 447−453.
40. De Groot, H. J. M. (2000) *Curr. Opin. Struct. Biol. 10*, 593−600.
41. Buss, V., Wiengart, O., and Sugihara, M. (2000) *Angew. Chem., Int. Ed. 39*, 2784−2786.
42. Kochendoerfer, G. G., Verdegem, P. J. E., Van der Hoef, I., Lugtenburg, J., and Mathies, R. A. (1996) *Biochemistry 35*, 16230−16240.
43. Kakatani, T., Akiyama, R., Hatano, Y., Imamoto, Y., Shichida, Y., Verdegem, P., and Lugtenburg, J. (1998) *J. Phys. Chem. B 102*, 1334−1339.
44. Spiesecke, H., and Schneider, W. G. (1961) *Tetrahedron Lett. 14*, 468−472.
45. Lauterbur, P. (1961) *J. Am. Chem. Soc. 83*, 1838−1846.
46. Tokuhiro, T., and Fraenkel, G. (1969) *J. Am. Chem. Soc. 91*, 5005−5013.
47. Pople, J. A., and Walmsley, S. H. (1962) *Mol. Phys. 5*, 15−20.
48. Su, W. P., Schrieffer, J. R., and Heeger, A. J. (1980) *Phys. Rev. B22*, 2099−2111.
49. Salaneck, W. R., Friend, R. H., and Bredas, J. L. (1999) *Phys. Rep. 319*, 231−251.
50. Peierls, R. E. (1955) in *Quantum theory of solids*, Oxford University Press, London.
51. Sterling, C. (1964) *Acta Crystallogr. 17*, 1224−1228.
52. Elia, G. R., Childs, R. F., Britten, J. F., Yang, D. S. C., and Santasiero, B. D. (1996) *Can. J. Chem. 74*, 591−601.
53. Lu, Y. (1988) in *Solitons & polarons in conducting polymers*, World Scientific Publishing, Singapore.

BI0023798